International Journal of Solids and Structures 64–65 (2015) 155–165

Contents lists available at ScienceDirect

International Journal of Solids and Structures

journal homepage: www.elsevier.com/locate/ijsolstr

Soft hands: An analysis of some gripping mechanisms in soft robot design

Xuance Zhou [a,*], Carmel Majidi [b], Oliver M. O'Reilly [a,*]

[a] Department of Mechanical Engineering, University of California at Berkeley, Berkeley, CA 94720, USA
[b] Department of Mechanical Engineering, Carnegie Mellon University, Pittsburgh, PA 15213, USA

ARTICLE INFO

Article history:
Received 12 October 2014
Received in revised form 23 March 2015
Available online 3 April 2015

Keywords:
Gripping
Soft robots
Robot hand
Rod theory
Elastica
Intrinsic curvature
Stability

ABSTRACT

In contrast to their more rigid counterparts, soft robots have the ability to gently grip and maneuver objects with open-loop kinematic control. Guided by several recent designs and implementations of soft robot hands, the present paper analyzes a rod-based model for the fingers in the hand of a soft robot. We show precisely how gripping is achieved and how the performance can be affected by varying the system's parameters. The designs we are interested in feature pneumatic control of the soft robot and we model this actuation as a varying intrinsic curvature profile of the rod. Our work provides a framework for the theoretical analysis of the soft robot and the resulting analysis can also be used to develop some design guidelines.

1. Introduction

Soft robots contain little or no rigid material and have been designed to perform a wide variety of robotic tasks, from bio-inspired crawling (Shepherd et al., 2011) and peristalsis (Seok et al., 2013) to pick-and-place gripping (Suzumori, 1996, Brown et al., 2010, Ilievski et al., 2011, Song and Sitti, 2014, Mosadegh et al., 2014, Deimel and Brock, 2014). Their unique promise for enabling inherently safe and adaptive contact with both solid and soft surfaces has made these emerging systems attractive for wearable and field robotics (Trivedi et al., 2008; Majidi, 2013; Kim et al., 2013; Laschi and Cianchetti, 2014). This is especially true of soft gripping mechanisms, which use a single end effector or multiple fingers and are dramatically more compliant than conventional robot grippers. For some designs, such as the four-fingered gripper (Suzumori, 1996) and six-pointed star gripper (Ilievski et al., 2011) shown in Fig. 1(a) and (b), gripping is achieved with pneumatic actuation. In contrast, the octopus-like soft robot shown in Fig. 1(c) uses an artificial tentacle that is actuated with motor-driven cables and shape memory alloy (Laschi et al., 2012). Soft robot gripping has also been demonstrated with bio-hybrid actuators composed of ventricular cardiomyocyte cells harvested on a thin film of silicone elastomer, as shown in Fig. 1(d) (Feinberg et al., 2007).

Compared to piecewise rigid gripping elements, the fingers or end effector of a soft gripper have low flexural rigidity and will bend during grasping tasks. This is most pronounced in grippers that conform to an object and make contact along a finite length, as is demonstrated in Fig. 1(b) and (c). In the case of angular objects (i.e., with straight edges), such "shape matching" is enhanced by adding a conformal sleeve to the actuator, which restricts bending to predefined joints (Galloway et al., 2013). Nonetheless, even in the case of soft grippers that only make point contact with an object, such as those in Fig. 1(a) and (d), bending can have a dramatic influence on control, contact force, and load bearing capability. As with conforming grippers, point-contact grippers have intrinsic flexural compliance that eliminates the need for fine kinematic control of the relative position of the end effector during unilateral contact with a fragile object. This compliance reduces the dependency on force-feedback control and prevents damage to the object in cases where the gripper overshoots.

The wealth of designs and implementations often renders it difficult to gain a perspective on how sufficient pressure is induced in the contact area between the soft hand finger and the workpiece. In order to examine this issue, we will develop and analyze a rod-based, flexible model for three different grips. Referring to Fig. 2, we consider a pair of fingers attached to a palm. The pair

* Corresponding authors. Tel.: +1 510 642 0877.
E-mail address: oreilly@berkeley.edu (O.M. O'Reilly).

http://dx.doi.org/10.1016/j.ijsolstr.2015.03.021
0020-7683/

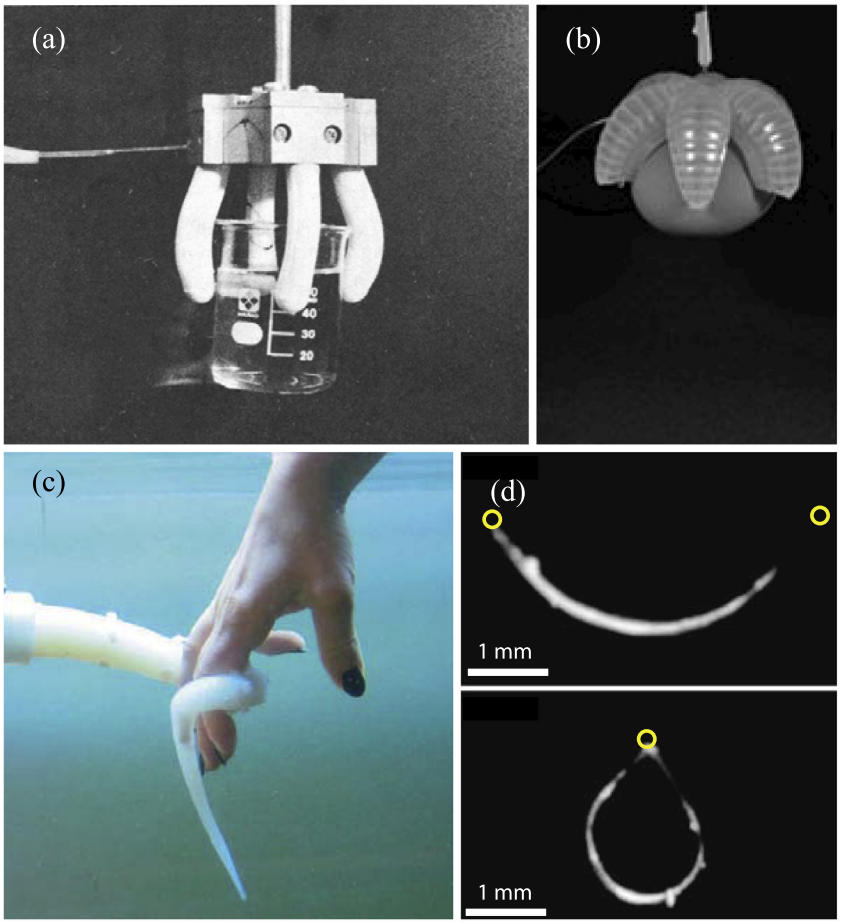

Fig. 1. Examples of soft robot hands. (a) Four-fingered pneumatic gripper from Suzumori (1996), six-pointed pneumatic star gripper from Ilievski et al. (2011), (c) octopus-like soft robot tentacle from Laschi and Cianchetti (2014), and (d) bio-hybrid pinching gripper from Feinberg et al. (2007).

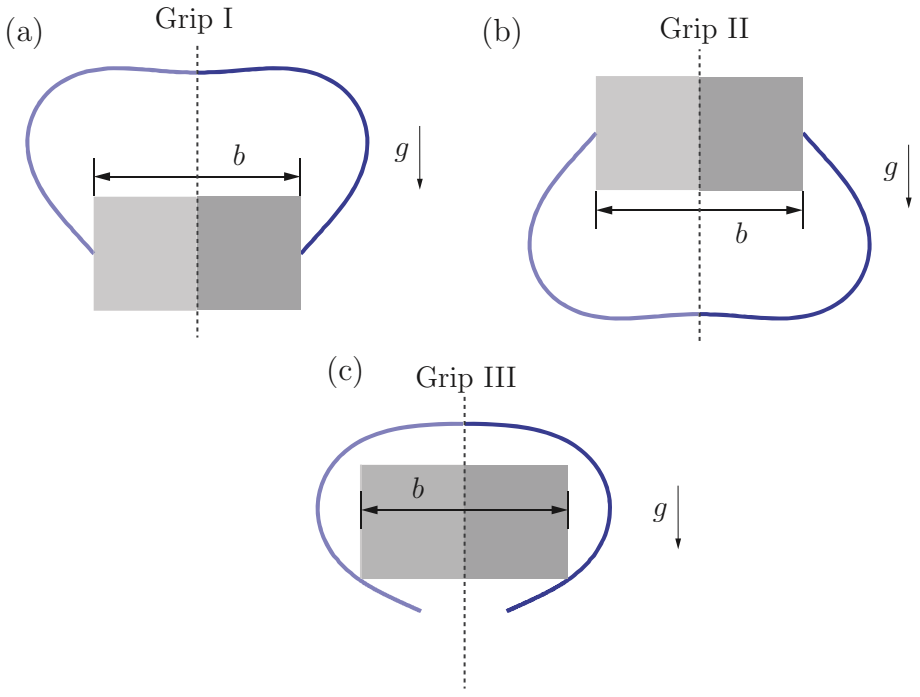

Fig. 2. Illustration of three typical gripping modes of a workpiece with the width b. In Grips I & II which are shown in (a) and (b), respectively, the workpiece is lifted with the help of static friction forces at the tip of the finger. In Grip III, which is shown in (c), the workpiece is lifted by the normal (pinching) force together with static friction forces at the contact point of the finger with the workpiece.

of rods modeling the figures are assumed to have a controllable intrinsic curvature $\kappa_g = \kappa_0(s)$. In particular, we seek to examine the influence of profiles $\kappa_0(s)$ on the gripping effectiveness. For simplicity, we assume the two rods share the same intrinsic curvature profile and are synchronized. Thus, by symmetry, it is sufficient to analyze a single rod. As shall be seen from our analysis, by appropriately varying κ_0, it is possible to change the normal force (or the pinching force) at the contact point of the payload with the finger and successfully induce a state of static Coulomb friction between the payload and the finger. Our modeling and analysis work builds on the earlier papers (Majidi et al., 2012, 2013; Zhou et al., 2015).

While we do not discuss the precise mechanism by which the intrinsic curvature is changed, there has been an increased interest in the development of mechanisms for changing κ_0 in components of soft robots. The interested reader is referred to Galloway et al. (2013), Shepherd et al. (2013), Suzumori et al. (2007), Takashima et al. (2011), Wakimoto et al. (2009) for examples of these mechanisms. Also, in order to make the theoretical model more tractable for analysis, we only examine gripping mechanisms that involve point contact with an object. As previously addressed for soft robot locomotion in our earlier work (Majidi et al., 2013), having an unknown length of contact ℓ_c between a flexible gripping element and object results in a free-boundary problem and introduces the need for an additional natural boundary condition. Moreover, point-contact may have practical advantages for pick-and-place due to lower stiction. This is especially true for grasping sticky objects or at small length scales where attractive forces (such as electrostatic, van der Waals, and capillary) become relatively significant. In these cases, conforming grippers that engage in finite contact may require greater detachment force to peel their soft fingers from the object.

The paper is organized as follows: In the next section, Section 2, models for the systems shown in Figs. 1 and 2 are established using rod theory. In particular, the governing equations for the configurations shown in Fig. 2 are established. In Section 3, numerical integrations of the governing equations are analyzed, and, with the help of a variational principle, the stability of the equilibrium configurations are discussed in Section 4. Our analyses demonstrate how varying the intrinsic curvature can control the gripping force and shape of the soft robot's hands in a manner that enables manipulation of the workpiece. We conclude the paper with a discussion on different intrinsic curvature profiles in Section 5 and a set of design recommendations for optimal performance of soft robot gripping devices featuring varying intrinsic curvature rods.

2. A simple model for a soft robot hand

To establish a feasible model for the gripping schemes shown in Fig. 2, we model the finger as an inextensible, perfectly flexible elastic rod. The rod theory we use is known as Euler's theory for the elastica. Referring to Fig. 3, the centerline of the rod is parameterized by an arc length coordinate $s \in [0, \ell]$ and the position of a point on the centerline is denoted by $\mathbf{r}(s)$. The rod is assumed to be uniform of length ℓ with a flexural rigidity EI, mass per unit length ρ, and an externally controlled intrinsic curvature profile $\kappa_g = \kappa_0(s)$. As discussed in Majidi et al. (2013), the pneumatic actuation system in some soft robots induce changes to EI and ρ but we do not consider these effects here.[1]

[1] Incorporating changes to EI and ρ into the model would follow the lines of similar developments in models for growing plant stems that are discussed in Faruk Senan et al. (2008) and O'Reilly and Tresierras (2011).

2.1. Background

The position of an arbitrary material point located at $s = s^*$ on the centerline of the rod has the representation

$$\mathbf{r}(s = s^*) = X(s = s^*)\mathbf{E}_1 + Y(s = s^*)\mathbf{E}_2, \tag{1}$$

where the Cartesian coordinates X and Y are defined by

$$\begin{aligned} X(s = s^*) &= X(s = 0) + \int_0^{s^*} \cos(\theta(\xi))\mathrm{d}\xi, \\ Y(s = s^*) &= Y(s = 0) + \int_0^{s^*} \sin(\theta(\xi))\mathrm{d}\xi, \end{aligned} \tag{2}$$

where ξ is a dummy variable. In (2), the angle θ is defined as the angle that the unit tangent vector $\mathbf{r}'$ makes with the horizontal $\mathbf{E}_1$ direction:

$$\mathbf{r}' = \cos(\theta(s))\mathbf{E}_1 + \sin(\theta(s))\mathbf{E}_2, \tag{3}$$

where the prime denotes the partial derivative with respect to s. We shall assume that $\mathbf{r}$ is continuous (i.e., there are no breaks in the rod). It follows that θ and $\mathbf{r}'$ will also be continuous (i.e., there are no kinks in the rod).

The jump in an arbitrary function $\mathcal{X} = \mathcal{X}(s, \theta(s), \theta'(s))$ at the point $s = \zeta$ is represented using a compact notation:

$$[\![\mathcal{X}]\!]_\zeta = \mathcal{X}(\zeta^+) - \mathcal{X}(\zeta^-), \tag{4}$$

where

$$\begin{aligned} \mathcal{X}(\zeta^-) &= \lim_{s \nearrow \zeta} \mathcal{X}(s, \theta(s), \theta'(s)), \\ \mathcal{X}(\zeta^+) &= \lim_{s \searrow \zeta} \mathcal{X}(s, \theta(s), \theta'(s)). \end{aligned} \tag{5}$$

Jumps in fields will be associated with points of application of forces at discrete points along the rod in the sequel.

The bending moment $\mathbf{M}$ in the rod is prescribed by a classic constitutive equation:

$$\mathbf{M} = EI(\theta' - \kappa_0)\mathbf{E}_3, \tag{6}$$

where κ_0 is a signed intrinsic curvature. In addition to a gravitational force $-\rho g\mathbf{E}_2$ per unit length and terminal loadings acting at the ends of the rod, we need to allow for the possibility of a singular force $\mathbf{F}_\gamma$ at $s = \gamma$. In the problem at hand, this force models the contact of the workpiece with the rod for the grip shown in Fig. 2(c). The governing equations for the rod can be obtained from balances of linear and angular momenta in a standard fashion:

$$\begin{aligned} &\mathbf{n}' - \rho g\mathbf{E}_2 = \mathbf{0}, \\ &\frac{d}{ds}(EI(\theta' - \kappa_0)) + n_2\cos(\theta) - n_1\sin(\theta) = 0, \\ &[\![\mathbf{n}]\!]_\gamma + \mathbf{F}_\gamma = \mathbf{0}. \end{aligned} \tag{7}$$

In the second of these balances, the contact force $\mathbf{n}$ has the representation $\mathbf{n} = n_1\mathbf{E}_1 + n_2\mathbf{E}_2$.

Henceforth, we develop models for three distinct configurations of the rod. In the first configuration, which is shown in Fig. 2(a), the end of the rod at $s = \ell$ is in point contact with the workpiece and a normal force together with a dry friction force is present at this interface. We refer to this configuration as Grip I. A closely related grip, Grip II, is shown in Fig. 2(b). In this configuration, the gripper is below the workpiece and again makes point contact at the tips of the two fingers. The third configuration of interest, which we refer to as Grip III, arises when the singular contact point is at $s = \gamma$ (cf. Fig. 2(c)). Examples of these configurations can be seen in Figs. 4 and 5. We now turn towards establishing the governing equations for the models for Grip I and Grip II.

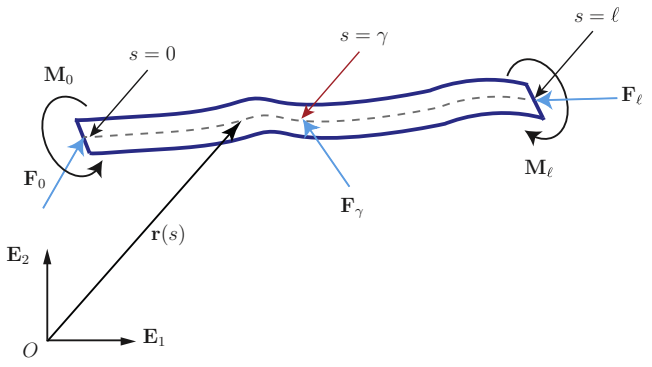

Fig. 3. Schematic representation of an elastica of length ℓ showing the position $\mathbf{r}$ of a point on the centerline. The rod is subject to a terminal force $\mathbf{F}_0$ and terminal moment $\mathbf{M}_0$ at $s=0$, a terminal force $\mathbf{F}_\ell$ and terminal moment $\mathbf{M}_\ell$ at the end $s=\ell$, and a force $\mathbf{F}_\gamma$ at the point $s=\gamma$.

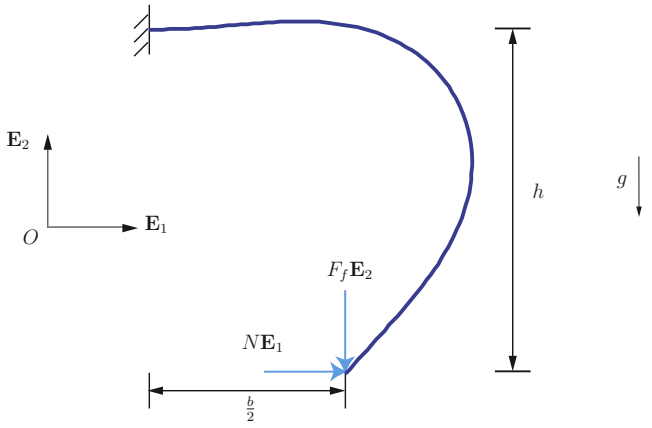

Fig. 4. Schematic of the model for Grip I. In this model, the workpiece is assumed to be held stationary by static friction at the point contact at the tip of the rod $s=\ell$: $\mathbf{F}_\ell = N\mathbf{E}_1 + F_f\mathbf{E}_2$.

2.2. Governing equations for Grips I and II

In Grip I, the workpiece is assumed to be held stationary with the help of static friction. We define the end point of the rod that connects to the palm or the other soft finger to be $s=0$ and the tip of the rod that touches the workpiece to be $s=\ell$. At the tip of the rod, a normal force $N\mathbf{E}_1$ and a friction force $F_f\mathbf{E}_2$ are assumed to act. The normal force $N\mathbf{E}_1$ ensures that the unilateral constraint

$$\int_0^\ell \cos(\theta(s))\mathrm{d}s = \frac{b}{2} \tag{8}$$

is enforced. Here, $b = 2((X(\ell) - X(0))$ is a constant width associated with the workpiece. It is easy to see that the friction force $F_f\mathbf{E}_2$ balances half the weight $2mg$ of workpiece, namely,

$$-F_f = mg. \tag{9}$$

The normal and friction forces need to satisfy the static friction criterion:

$$|F_f| \leqslant \mu_s N, \tag{10}$$

where μ_s is a coefficient of static friction.

We recall that the total energy of the rod consists of the sum of the strain energy, gravitational potential energy and the potential energy of the terminal load $\mathbf{F}_\ell = N\mathbf{E}_1 + F_f\mathbf{E}_2$:

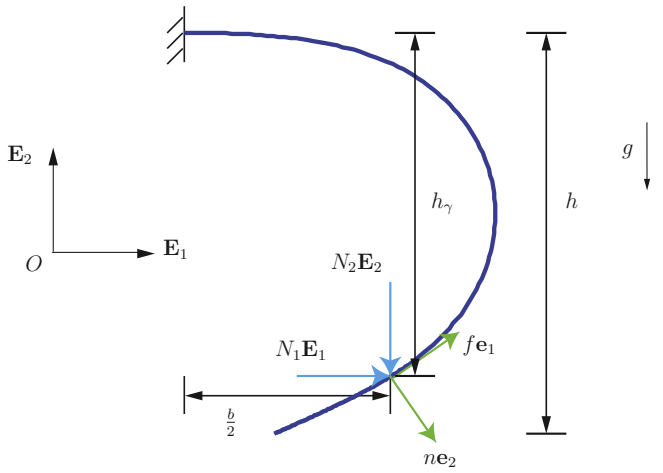

Fig. 5. Schematic of the model for Grip III. Here, point contact of the workpiece and the rod occurs at the point $s=\gamma$. The workpiece is assumed to be held stationary by a normal force $n\mathbf{e}_2$ along with a static friction force $f\mathbf{e}_1$. For the case shown, $N_2 < 0$ and $f < 0$.

$$V = \int_0^\ell \left\{ \frac{EI}{2}(\theta' - \kappa_0)^2 + \rho g Y(s) - \mathbf{F}_\ell \cdot \mathbf{r}' \right\} \mathrm{d}s. \tag{11}$$

The integral can be simplified using a standard change in the order of integration (see Farjoun and Neu (2005)):

$$\int_0^\ell \rho g Y(s)\mathrm{d}s = \int_0^\ell \rho g(\ell - s)\sin(\theta(s))\mathrm{d}s, \tag{12}$$

where $Y(0) = 0$. As we are assuming that both ends of the rod are fixed, (7) or, equivalently, the first variation of V, can be used to derive the boundary-value problem for the deformed shape $\theta = \theta^*$ of the rod:

$$EI(\theta'' - \kappa_0') - \rho g(\ell - s)\cos(\theta) + F_f\cos(\theta) - N\sin(\theta) = 0, \quad s \in (0, \ell). \tag{13}$$

In addition, the sought-after solution $\theta = \theta^*$ needs to satisfy the boundary conditions

$$\theta(0) = 0, \quad \theta'(\ell) = \kappa_0(\ell), \quad \int_0^\ell \cos(\theta(s))\mathrm{d}s = \frac{b}{2} \tag{14}$$

and the static friction criterion (10).

The corresponding developments for Grip II follow in a straightforward manner and, in the interests of brevity, are not explicitly discussed here.

2.3. Governing equations for Grip III

In Grip III, the corner of the work piece is assumed to be in point contact with the rod from at $s=\gamma$. In an effort to facilitate the discussion, we define two new unit vectors:

$$\begin{aligned} \mathbf{e}_1 &= \cos(\theta(\gamma))\mathbf{E}_1 + \sin(\theta(\gamma))\mathbf{E}_2, \\ \mathbf{e}_2 &= -\sin(\theta(\gamma))\mathbf{E}_1 + \cos(\theta(\gamma))\mathbf{E}_2. \end{aligned} \tag{15}$$

Here, $\mathbf{e}_1$ is tangent to the centerline of the rod at $s=\gamma$ while $\mathbf{e}_2 = \mathbf{E}_3 \times \mathbf{e}_1$ is normal to the centerline of the rod at $s=\gamma$. With the help of $\mathbf{e}_1$ and $\mathbf{e}_2$, the normal force n and its corresponding friction force f_f acting as $s=\gamma$ are related to the force components N_1 and N_2 as follows:

$$\mathbf{F}_\gamma = f\mathbf{e}_1 + n\mathbf{e}_2 = N_1\mathbf{E}_1 + N_2\mathbf{E}_2. \tag{16}$$

We emphasize that the static friction criterion at $s=\gamma$ is

$$|f| \leqslant \mu_s n. \tag{17}$$

To examine the effects of $\mathbf{F}_\gamma$ on the equilibrium configuration of the rod, we apply (7) to the segment $s \in (\gamma, \ell)$ and conclude that

$$\begin{aligned} &\mathbf{n}(\gamma^+) = -\rho g(\ell-\gamma)\mathbf{E}_2, \\ &\mathbf{n}(\gamma^-) = N_1\mathbf{E}_1 + N_2\mathbf{E}_2 - \rho g(\ell-\gamma)\mathbf{E}_2. \end{aligned} \tag{18}$$

Using the second of these results, it is straightforward to establish an expression for the potential energy V of the rod:

$$\begin{aligned} V = &\int_0^\gamma \left\{\frac{EI}{2}(\theta'-\kappa_0)^2 + \rho g Y(s) - \mathbf{n}(\gamma^-)\cdot\mathbf{r}'\right\}\mathrm{d}s \\ &+ \int_\gamma^\ell \left\{\frac{EI}{2}(\theta'-\kappa_0)^2 + \rho g Y(s)\right\}\mathrm{d}s, \end{aligned} \tag{19}$$

where

$$Y(s) = \int_0^s \sin(\theta(\xi))\mathrm{d}\xi. \tag{20}$$

In establishing (19) we emphasize that we are ignoring inertia effects.

As with Grips I and II, either a first variation of V can be performed or (7) can be used to establish the boundary-value problem which is used to determine the deformed shape θ^* of the rod:

$$\begin{aligned} &EI(\theta''-\kappa_0') - \rho g(\ell-s)\cos(\theta) = 0, \quad s\in(0,\gamma), \\ &EI(\theta''-\kappa_0') - \rho g(\ell-s)\cos(\theta) + N_2\cos(\theta) \\ &- N_1\sin(\theta) = 0, \quad s\in(\gamma,\ell). \end{aligned} \tag{21}$$

Here, the solution $\theta=\theta^*$ satisfies the conditions

$$\begin{aligned} &\theta(0)=0, \quad \theta'(\ell)=\kappa_0(\ell), \quad \int_0^\gamma \cos(\theta(s))\mathrm{d}s = \frac{b}{2}, \\ &[\![\theta]\!]_\gamma = 0, \quad [\![\theta']\!]_\gamma = 0, \end{aligned} \tag{22}$$

in addition to the static friction criterion (17). In our formulation of the governing equations, we have tacitly assumed that the tip of the rod will not touch the workpiece. Thus,

$$h_\gamma < h. \tag{23}$$

3. The gripping mechanism

3.1. Intrinsic curvature profile and dimensionless parameters

In our work, gripping is controlled by varying the intrinsic curvature profile and the choice of this profile is critical. For the purposes of discussion, we start with the simplest possible intrinsic curvature profile: that of a constant intrinsic curvature profile. The behavior of a clamped-free rod loaded by its own weight and endowed with the constant intrinsic curvature profile $\kappa_g=\kappa_0$ is shown in Fig. 6. This figure is used to show that the intrinsic curvature profile does not generate physically unrealistic self-intersections of the rod as κ_0 is varied.

For the numerical simulations to be carried out in the sequel, it is convenient to define a dimensionless flexural rigidity D, mass M, intrinsic curvature parameter, and arc-length parameter:

$$D = \frac{EI}{\rho g \ell^3}, \quad M = \frac{m}{\rho\ell}, \quad \bar\kappa_0 = \ell\kappa_0, \quad \bar s = \frac{s}{\ell}. \tag{24}$$

We also use the weight $\rho g\ell$ of the rod to non-dimensionalize the friction and normal forces.

3.2. Grip I

We start by considering the tip of the rod in point contact with the workpiece as shown in Fig. 4 which is the most common gripping mode either for a robot or a human being. A key to successful gripping is to produce a pinching force N_1 at the contact point so the weight of the workpiece can be supported without the static friction criterion being violated. To see how this can be achieved by varying $\bar\kappa_0$, we solve the boundary value problem given by (13) and (14) to determine the deformed shape of the rod and the dimensionless normal $\frac{N_1}{\rho g\ell}$ and the correspond maximum static friction $\frac{\mu_s N_1}{\rho g\ell}$ forces.

As can be seen from Fig. 7(a), as $-\bar\kappa_0$ increases, eventually a point is reached where the weight $-2mg\mathbf{E}_2$ of the workpiece can be balanced by the static friction. One thing to notice is that the relationship between height of the rod tip h of the finger and the magnitude $|\bar\kappa_0|$ of the intrinsic curvature in the feasible region is almost linear in Fig. 7(c). This property may facilitate control of the gripping mechanism.

Beyond the ability of the soft hand to grip the workpiece with the palm pointing down (as shown in Fig. 2(a) and discussed in Fig. 7), it is also of interest to see whether the soft hand can hold an object with the palm pointing upwards. As can be seen from Fig. 8, as $-\bar\kappa_0$ increases, the weight of the workpiece can be supported by the static friction force at the contact point of the rod and the workpiece. One feature worth mentioning is that, for the same value of $|\bar\kappa_0|$, the normal force N_1 with the palm pointing up is higher than that with the palm pointing down. The difference can be attributed to the self weight of the rod: with the palm pointing up, the rod's weight can increase the curvature which produces an increased normal force N_1. The stability of the equilibrium configurations, which is usually a challenge for an inverted rod, will shortly be discussed in Section 4.

3.3. Grip III

Grip III, where the work piece is cradled by the fingers, requires a more delicate analysis than either Grips I or II. Referring to Fig. 9,

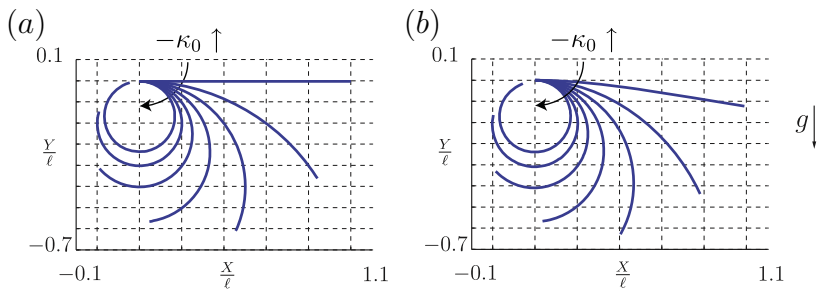

Fig. 6. Features of the constant intrinsic curvature profile of a clamped-free rod as the constant κ_0 is varied. (a) The corresponding deformed shape of a rod with a constant intrinsic curvature profile. (b) The corresponding deformed shape of a heavy rod with a constant intrinsic curvature profile and a vertical gravity loading. The dimensionless flexural rigidity D of the rod is $D=\frac{EI}{\rho g\ell^3}=1$.

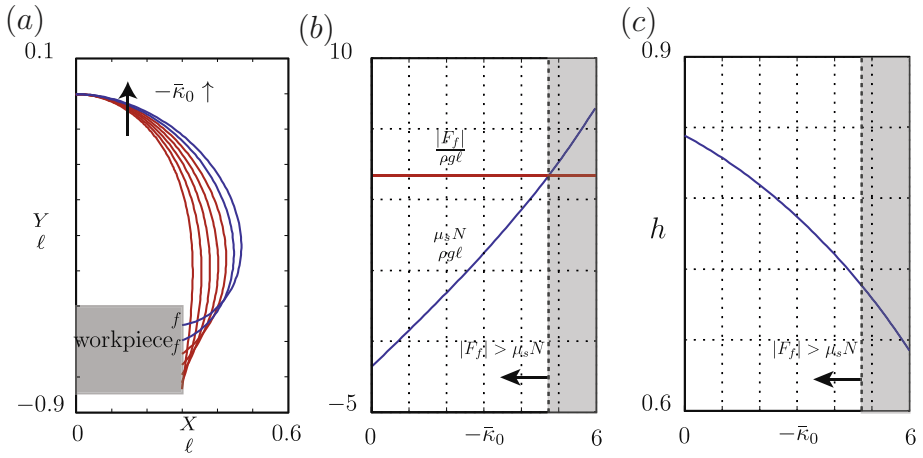

Fig. 7. Grip I of the soft hand. (a) The deformed shape of the soft hand as $\bar{\kappa}_0$ varies with the pair of feasible configurations labeled *f*. (b) The corresponding dimensionless friction $\frac{|F_f|}{\rho g \ell}$ required and the maximum friction $\frac{\mu_s N}{\rho g \ell}$ that can be provided. (c) The height h of the tip of the rod. The shaded regions in (b) and (c) indicates the feasible regions for Grip I. For the results shown, $\frac{b}{\ell} = 0.6$, $D = \frac{EI}{\rho g \ell^3} = 1$, $\mu_s = 1$, $M = 5$ and $-\bar{\kappa}_0$ increases from 0 to 6.

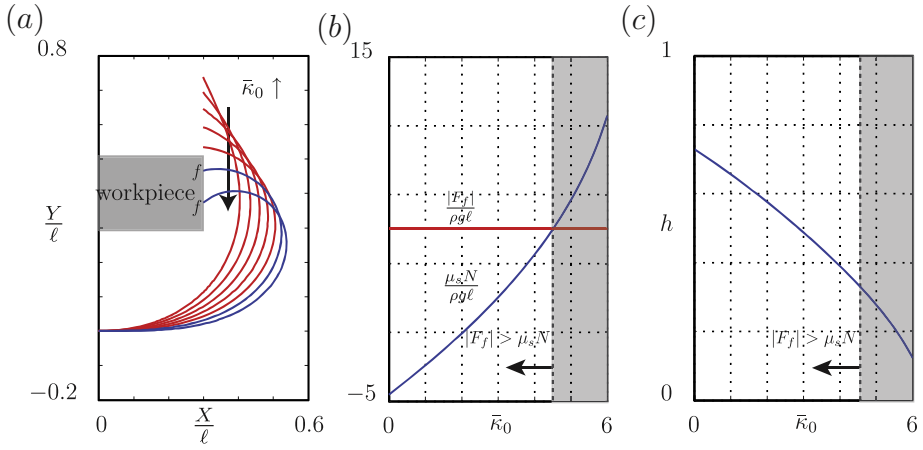

Fig. 8. Grip II of the soft hand. (a) The deformed shape of the soft hand as $\bar{\kappa}_0$ varies with the pair of feasible configurations labeled with *f*. (b) The corresponding dimensionless friction $\frac{|F_f|}{\rho g \ell}$ required and the maximum friction $\frac{\mu_s N}{\rho g \ell}$ that can be provided. (c) The height h of the tip of the rod. The shaded regions in (b) and (c) indicates the feasible regions for Grip II. For the results shown, $\frac{b}{\ell} = 0.6$, $D = \frac{EI}{\rho g \ell^3} = 1$, $\mu_s = 1$, $M = 5$, and $\bar{\kappa}_0$ increases from 0 to 6.

we find for the soft hand to hold an object, the magnitude of the intrinsic curvature must be within a given range. If $-\bar{\kappa}_0$ is too small, then the shear force n_2 will be small which leads to a violation of the static friction criterion (17). However, if $-\bar{\kappa}_0$ is too large, then the force n_1 will be quite large which also leads to the violation of (17). As shown in Fig. 9(c), a large $-\bar{\kappa}_0$ can induce a curled-up tip and could result in the violation of (23).

4. Stability analysis

The equilibrium configurations of the rod discussed in Section 3 feature large deformations and it is prudent to examine if the configurations are stable (i.e., there are no buckling instabilities). The presence of the isoperimetric constraint is accommodated by discretizing the system and performing an appropriate eigenvalue analysis.

4.1. Stability analysis for Grips I and II

As illustrated by Fig. 10, the rod is divided into a set of K segments of length ds, the system can be parameterized by $K+1$ variables $\theta_0, \ldots, \theta_K$. The total potential energy (11) is approximated by its discrete counterpart:

$$
\begin{aligned}
V_{\text{dis}} = {} & \frac{EI}{2}\sum_{i=1}^{K}\left(\frac{\theta_i - \theta_{i-1}}{ds} - \kappa_0\right)^2 ds + \rho g(\ell - s_0)\sin(\theta_0)\frac{ds}{2} \\
& + \sum_{i=1}^{K-1}\rho g(\ell - s_i)\sin(\theta_i) ds + \rho g(\ell - s_K)\sin(\theta_K)\frac{ds}{2} \\
& - F_f \sin(\theta_0)\frac{ds}{2} - F_f\sum_{i=1}^{K-1}\sin(\theta_i) d - F_f\sin(\theta_K)\frac{ds}{2} - N\cos(\theta_0)\frac{ds}{2} \\
& - N\sum_{i=1}^{K-1}\cos(\theta_i) ds - N\cos(\theta_K)\frac{ds}{2}.
\end{aligned}
$$

The isoperimetric constraint is also discretized and we need to consider boundary conditions on θ_i:

$$
\begin{aligned}
& \cos(\theta_0)\frac{ds}{2} + \sum_{i=1}^{K-1}\cos(\theta_i) ds + \cos(\theta_K)\frac{ds}{2} = \frac{b}{2}, \\
& \theta_0 = 0, \qquad \frac{\theta_{K+1} - \theta_{K-1}}{2ds} = \kappa_0(\ell)
\end{aligned}
\tag{26}
$$

The two Eq. $(26)_{2,3}$ can be directly imposed on (25) to reduce the dimension of the discretized system:

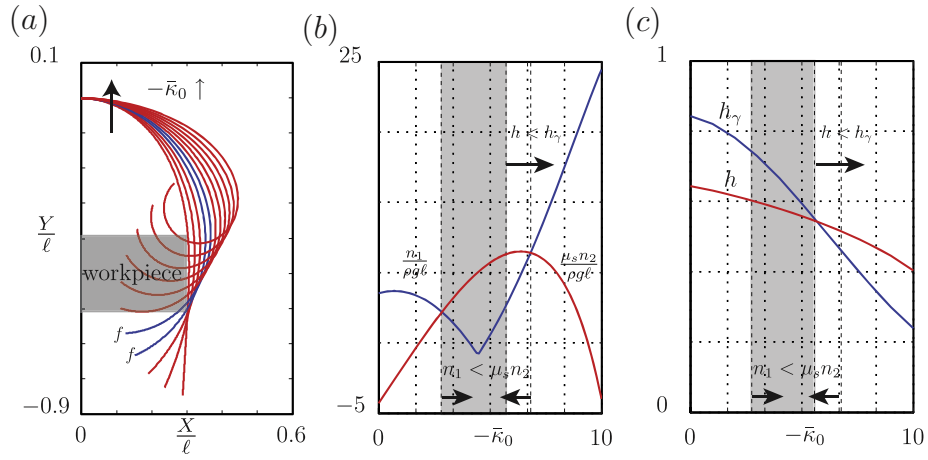

Fig. 9. Grip III of the soft hand holding a given workpiece. (a) The deformed shape of the soft hand as $\bar{\kappa}_0$ varies with the pair of feasible configurations labeled *f*. (b) The corresponding dimensionless friction force $\frac{n_1}{\rho g \ell^3}$ needed and the maximum friction force $\frac{\mu_s n_2}{\rho g \ell^3}$ that can be provided. (c) The heights h and h_γ. The shaded regions in (b) and (c) are the feasible regions for Grip III. For the results shown, $\frac{\gamma}{\ell} = 0.8$, $\frac{b}{\ell} = 0.6$, $D = \frac{EI}{\rho g \ell^3} = 1$, $\mu_s = 1$, $M = 5$, and $-\bar{\kappa}_0$ increases from 0 to 10.

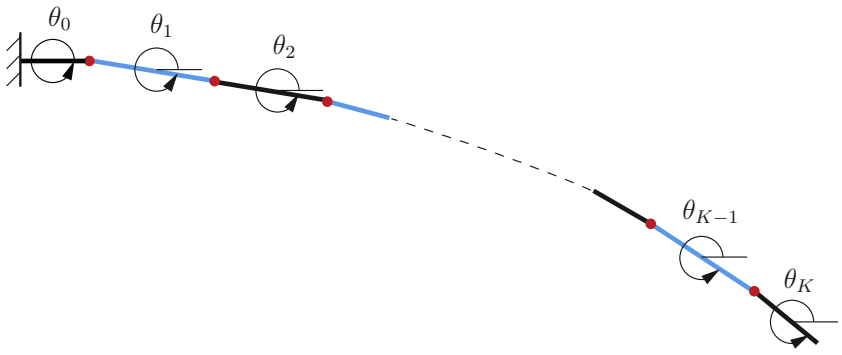

Fig. 10. Schematic of the discretization scheme for the rod.

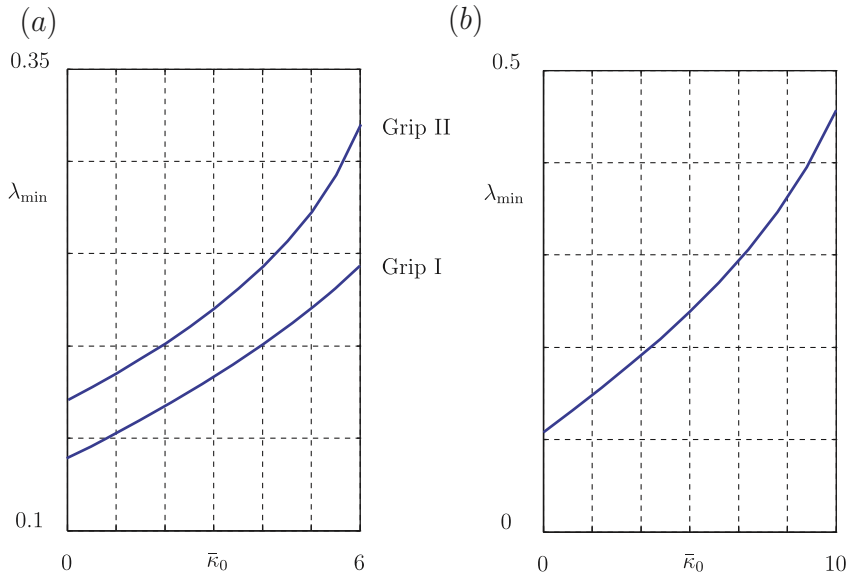

Fig. 11. (a) Verification of the stability of the equilibrium configuration shown in Figs. 7 and 8 by examining the minimum eigenvalue $\lambda_{\min}$ of L in an appropriate tangent subspace. (b) Verification of the stability of the equilibrium configuration shown in Fig. 9 (i.e., Grip III); For the results shown, $\frac{b}{\ell} = 0.6$, $D = \frac{EI}{\rho g \ell^3} = 1$, $M = 5$, and $\mu_s = 1$.

$$V_{\text{dis}} = \frac{EI}{2}\sum_{i=1}^{K}\left(\frac{\theta_i-\theta_{i-1}}{\mathrm{d}s}-\kappa_0\right)^2 \mathrm{d}s + \sum_{i=1}^{K-1}\rho g(\ell - s_i)\sin(\theta_i)\mathrm{d}s + \rho g(\ell - s_K)\sin(\theta_K)\frac{\mathrm{d}s}{2} - F_f\sum_{i=1}^{K-1}\sin(\theta_i)\mathrm{d}s - F_f\sin(\theta_K)\frac{\mathrm{d}s}{2} - N\frac{\mathrm{d}s}{2} - N\sum_{i=1}^{K-1}\cos(\theta_i)\mathrm{d}s - N\cos(\theta_K)\frac{\mathrm{d}s}{2} \tag{27}$$

subject to the constraint function c (from $(26)_1$):

$$c = \frac{\mathrm{d}s}{2} + \sum_{i=1}^{K-1}\cos(\theta_i)\mathrm{d}s + \cos(\theta_K)\frac{\mathrm{d}s}{2} - \frac{b}{2}. \tag{28}$$

We observe that the pair of functions V_{dis} and c depend on the states $\theta_1,\ldots,\theta_K$.

We next seek minimizers of V_{dis} which satisfy the discretized constraint (28). The extremizer, which can be found in a standard manner using the method of Lagrange multipliers, is denoted by $(\theta_1^*,\ldots,\theta_K^*)$. To examine the stability of the equilibrium state, it is convenient to define three $(K\times K)$ matrices:

$$\begin{aligned}\mathsf{F} &= \nabla^2 V_{\text{dis}}(\theta_1^*,\ldots,\theta_K^*),\\ \mathsf{H} &= \nabla^2 c(\theta_1^*,\ldots,\theta_K^*),\\ \mathsf{L} &= \mathsf{F} + \chi\mathsf{H}.\end{aligned} \tag{29}$$

Here, the Lagrange multiplier χ corresponds to contributions from the normal force $\chi\mathbf{E}_1 = N\mathbf{E}_1$ at the tip $s=\ell$ of the rod. It is well known that for an equilibrium to be stable, the potential energy has to be locally minimized. To check whether the equilibrium $(\theta_1^*,\ldots,\theta_K^*)$ locally minimizes Eq. (27), we use the classic method discussed in Luenberger and Ye (2008) of checking the eigenvalues of L corresponding to the eigenvectors of L that lie in the (K-1)-dimensional tangent subspace $\mathcal{M}$ that is orthogonal to the (K-dimensional) gradient vector $\nabla c\in\mathbb{R}^K$ defined by the discretized constraint (28). That is,

$$\mathcal{M} = \{\mathsf{u}\in\mathbb{R}^K : \nabla c(\theta_1^*,\ldots,\theta_K^*)\cdot\mathsf{u} = 0\}. \tag{30}$$

We denote an orthogonal basis for $\mathcal{M}$ by the set of K-dimensional vectors $\{\mathsf{u}_1,\ldots,\mathsf{u}_{K-1}\}$. This basis can be used to define a projection operator E where $\mathsf{Ez}\in\mathcal{M}$ for all $\mathsf{z}\in\mathbb{R}^K$:

$$\mathsf{E} = [\mathsf{u}_1,\ldots,\mathsf{u}_{K-1}]. \tag{31}$$

With the help of E, the stability of the equilibrium can be established by showing that the smallest eigenvalue of $\mathsf{E}^T\mathsf{LE}$ is strictly positive. As indicated by the results shown in Fig. 11(a), the quasistatic equilibrium configurations for Grips I and II satisfy the stability criterion.

4.2. Stability analysis for Grip III

For the case of Grip III, we define the discretized point which contact the object is *I*. Thus the discretized potential energy function reduces to

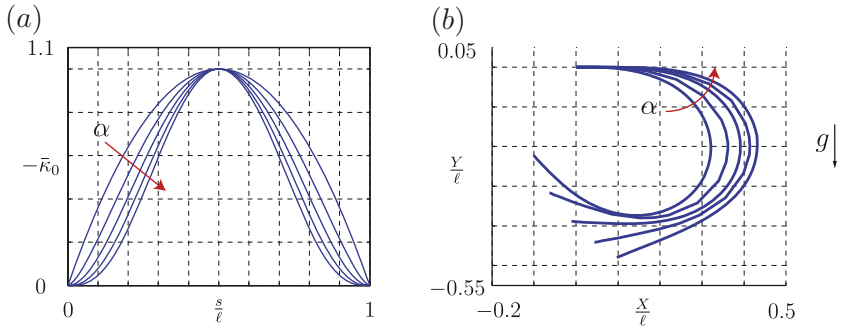

Fig. 12. Features of the curvature profile given by (34) as the parameter α is varied. (a) The dimensionless intrinsic curvature throughout the deformed rod. (b) The corresponding deformed shape of a heavy rod with an intrinsic curvature profile (34). For the results shown, $\bar{\kappa}_{\max}=6$, $p=-1$, and $D=\frac{EI}{\rho g\ell^3}=1$.

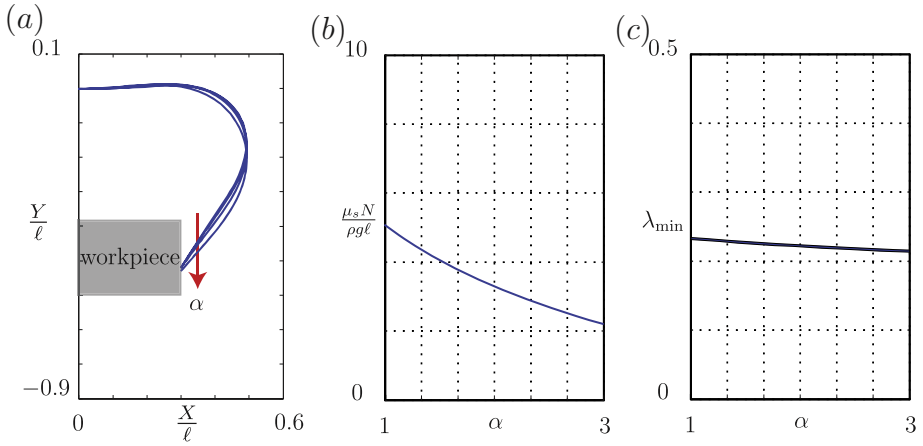

Fig. 13. Grip I of the soft hand where the workpiece faces downwards. (a) The deformed shape of the soft hand as α varies. (b) The corresponding maximum dimensionless friction force $\frac{\mu_s N}{\rho g\ell}$ that can be provided, (i.e., the loading bearing capacity). (c) Verification of the stability of the equilibrium configuration obtained by examining the minimum eigenvalue $\lambda_{\min}$ of L in an appropriate tangent subspace. For the results shown, $\frac{b}{\ell}=0.6, D=\frac{EI}{\rho g\ell^3}=1$, $\mu_s=1$, $\bar{\kappa}_{\max}=6$, $M=5$, and α increases from 1 to 3.

$$V_{\text{dis}} = \frac{EI}{2}\sum_{i=1}^{K}\left(\frac{\theta_i-\theta_{i-1}}{\mathrm{d}s}-\kappa_0\right)^2\mathrm{d}s+\rho g(\ell-s_0)\sin(\theta_0)\frac{\mathrm{d}s}{2}$$
$$+\sum_{i=1}^{K-1}\rho g(\ell-s_i)\sin(\theta_i)\mathrm{d}s+\rho g(\ell-s_K)\sin(\theta_n)\frac{\mathrm{d}s}{2}$$
$$-N_1\cos(\theta_0)\frac{\mathrm{d}s}{2}-N_1\sum_{i=1}^{I-1}\cos(\theta_i)\mathrm{d}s-N_1\cos(\theta_I)\frac{\mathrm{d}s}{2}$$
$$-N_2\sin(\theta_0)\frac{\mathrm{d}s}{2}-N_2\sum_{i=1}^{I-1}\sin(\theta_i)\mathrm{d}s-N_2\sin(\theta_I)\frac{\mathrm{d}s}{2}. \tag{32}$$

Subject to the constraint function c:

$$c=\frac{\mathrm{d}s}{2}+\sum_{i=1}^{I-1}\cos(\theta_i)\mathrm{d}s+\cos(\theta_I)\frac{\mathrm{d}s}{2}-\frac{b}{2} \tag{33}$$

We now follow the same procedure as we did for Grips I and II, but with a minor change in the objective function V_{dis} and constraint function c. Our numerical results can be seen in Fig. 11(b) and we conclude that the equilibrium configuration for Grip III satisfies the stability criterion.

5. The role of the intrinsic curvature profile

The constant intrinsic curvature profile κ_0 analyzed in the previous sections can be considered as too simplistic. Indeed, recent attention that has been paid to the mechanism of varying κ_0 throughout the soft robot (see, e.g., Galloway et al. (2013), Shepherd et al. (2013), Suzumori et al. (2007), Takashima et al. (2011), Wakimoto et al. (2009)), typically produce an intrinsic curvature profile which is non-uniform. It is clearly of interest to examine how robust the conclusions drawn in Sections 3 and 4 are to changes in the intrinsic curvature profile. To examine this issue, we consider the following intrinsic curvature profile:

$$\bar{\kappa}_0(\bar{s})=\mathrm{p}\bar{\kappa}_{\max}(4\bar{s}(1-\bar{s}))^{\alpha}, \tag{34}$$

with $\mathrm{p}=-1$ when the soft hand is pointing downwards, $\mathrm{p}=1$ when the soft hand is pointing upwards. The intrinsic curvature profile is such that $\bar{\kappa}_{\max}$ is the maximum intrinsic curvature in the rod and α regulates the degree of intrinsic curvature concentration as shown in Fig. 12.

For all three gripping configurations, the representative results shown in Figs. 13–15 illustrate that a concentrated intrinsic curvature profile will not increase the soft hand's gripping ability compared to the uniform case. In addition, the stability properties are

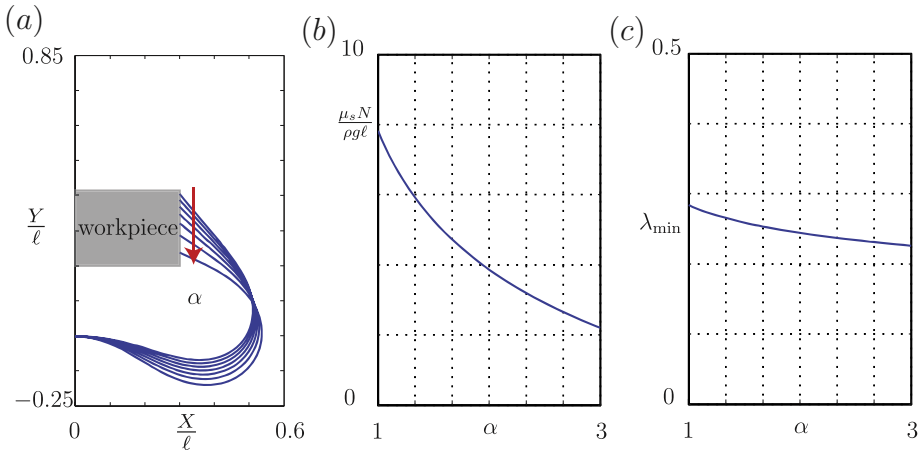

Fig. 14. Grip II of the soft hand where the workpiece points upwards. (a) The deformed shape of the soft hand as α varies. (b) The corresponding maximum dimensionless friction force $\frac{\mu_s N}{\rho g \ell}$ that can be provided, (i.e., the loading bearing capacity). (c) Verification of the stability of the equilibrium configuration obtained by examining the minimum eigenvalue $\lambda_{\min}$ of L in an appropriate tangent subspace. For the results shown, $\frac{b}{\ell}=0.6,\ D=\frac{EI}{\rho g \ell^3}=1,\ \mu_s=1,\ \bar{\kappa}_{\max}=6,\ M=5$, and α increases from 1 to 3.

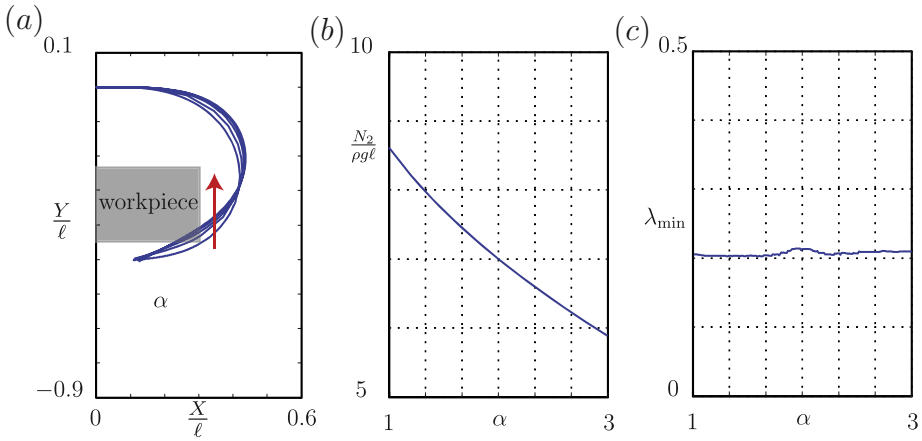

Fig. 15. Grip III of the soft hand holding a given workpiece. (a) The deformed shape of the soft hand as α varies. (b) The corresponding maximum force $\frac{N_2}{\rho g \ell}$ that can be provided (i.e., the load bearing capacity). (c) Verification of the stability of the equilibrium configuration obtained by examining the minimum eigenvalue $\lambda_{\min}$ of L in an appropriate tangent subspace. For the results shown, $\frac{b}{\ell}=0.6,\ D=\frac{EI}{\rho g \ell^3}=1,\ \mu_s=1,\ \bar{\kappa}_{\max}=6,\ M=5$, and α increases from 1 to 3.

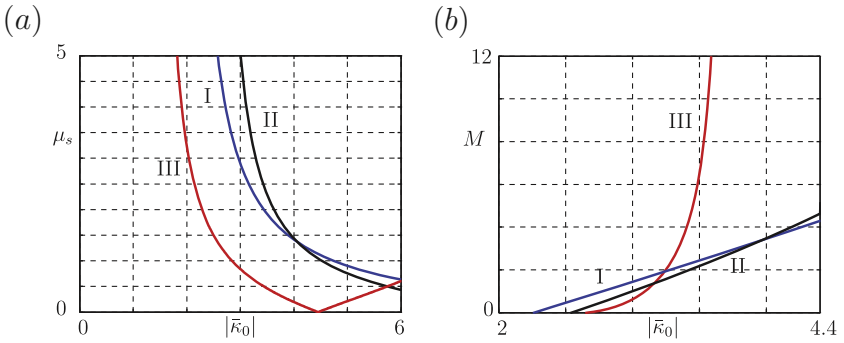

Fig. 16. (a) Given a workpiece with $M = 5$, the least μ_s required to successfully grip an object. (b) Given a static friction coefficient $\mu_s = 1$, the maximum workpiece weight M that can be accommodated. For the results shown, $\frac{b}{\ell} = 0.6$ and $D = \frac{EI}{\rho g \ell^3} = 1$.

not drastically different from the uniform intrinsic curvature profile considered earlier. These results are reassuring because in practice the actually profile is likely to be a combination of the constant intrinsic curvature and concentrated intrinsic curvature profiles.

6. Conclusions

In closing this paper, it is interesting to compare the loading capabilities of the three gripping configurations. To this end, we consider a uniform intrinsic curvature profile and first consider the minimum amount of static friction needed to lift a fixed mass M. The results are shown in Fig. 16(a). As expected, Grip III is superior in that it can transport the load with a smaller intrinsic curvature profile. We also note that for a particular value of $\bar{\kappa}_0$, no static friction is needed. In this case, the slope of the rod at the contact point with the workpiece and the $\mathbf{E}_2$ component of the normal force $n\mathbf{e}_2$ are such that $n\mathbf{e}_2 \cdot \mathbf{E}_2 = mg$. As m decreases, the critical value of $\bar{\kappa}_0$ where this situation occurs decreases. For the second set of numerical experiments, we fix the available μ_s and examine the largest load that can be carried. As shown in Fig. 16(b), Grip III has superior load bearing capabilities and shows a larger sensitivity to changes in $\bar{\kappa}_0$.

Based on the numerical simulations and analysis of the simple models for Grips I–III, the following conclusions on gripping can be drawn for the single-point gripping schemes:

1. In the gripping schemes, controlling the magnitude of the intrinsic curvature is sufficient to control the pinching force.
2. Concentration of intrinsic curvature does not significantly improve the effectiveness of the gripping.
3. Grip III, as expected, has superior load bearing capabilities.

While the design and operation of soft robot gripping devices also includes actuator technology, materials, and geometric dimensions required to deliver an effective gripping, it is hoped that the analyses presented in this paper can help to develop and enable design guidelines.

Acknowledgments

Support from a Defense Advanced Research Projects (DARPA) 2012 Young Faculty Award to Carmel Majidi is gratefully acknowledged. Xuance Zhou is grateful for the support of an Anselmo Macchi Fellowship for Engineering Graduate Students and a J.K. Zee Fellowship.

References

Brown, E., Rodenberg, N., Amend, J., Mozeika, A., Steltz, E., Zakin, M.R., Lipson, H., Jaeger, H.M., 2010. Universal robotic gripper based on the jamming of granular material. Proc. Nat. Acad. Sci. (U.S.A.) 107 (44), 18809–18814. http://dx.doi.org/10.1073/pnas.1003250107.

Deimel, R., Brock, O., 2014. A novel type of compliant, underactuated robotic hand for dexterous grasping. In: Robotics: Science and Systems (RSS). <http://www.robotics.tu-berlin.de/fileadmin/fg170/Publikationenpdf/deimel-14-RSS-draft.pdf>.

Farjoun, Y., Neu, J., 2005. The tallest column: a dynamical system approach using a symmetry solution. Stud. Appl. Math. 115 (3), 319–337. http://dx.doi.org/10.1111/j.1467-9590.2005.00316.x.

Faruk Senan, N.A., O'Reilly, O.M., Tresierras, T.N., 2008. Modeling the growth and branching of plants: a simple rod-based model. J. Mech. Phys. Solids 56 (10), 3021–3036. http://dx.doi.org/10.1016/j.jmps.2008.06.005.

Feinberg, A.W., Feigel, A., Shevkoplyas, S.S., Sheehy, S., Whitesides, G.M., Parker, K.K., 2007. Muscular thin films for building actuators and powering devices. Science 317, 1366–1370. http://dx.doi.org/10.1126/science.1146885.

Galloway, K., Polygerinos, P., Walsh, C., Wood, R., 2013. Mechanically programmable bend radius for fiber-reinforced soft actuators. In: 16th International Conference on Advanced Robotics (ICAR), 1–6. doi: 10.1109/ICAR.2013.6766586.

Ilievski, F., Mazzeo, A.D., Shepherd, R.F., Chen, X., Whitesides, G.M., 2011. Soft robotics for chemists. Angew. Chem. 123 (8), 1930–1935. http://dx.doi.org/10.1002/anie.201006464.

Kim, S., Laschi, C., Trimmer, B., 2013. Soft robotics: a bioinspired evolution in robotics. Trends Biotechnol. 31, 287–294. http://dx.doi.org/10.1016/j.tibtech.2013.03.002.

Laschi, C., Cianchetti, M., 2014. Soft robotics: new perspectives for robot body and control. Front. Bioeng. Biotechnol. 2 (3). http://dx.doi.org/10.3389/fbioe.2014.00003.

Laschi, C., Cianchetti, M., Mazzolai, B., Margheri, L., Folladore, M., Dario, P., 2012. Soft robot arm inspired by the octopus. Adv. Rob. 26 (7), 709–727. http://dx.doi.org/10.1163/156855312X6263437.

Luenberger, D.G., Ye, Y., 2008. Linear and nonlinear programming. International Series in Operations Research & Management Science,, Springer, New York (p. 116).

Majidi, C., 2013. Soft robotics: a perspective – current trends and prospects for the future. Soft Rob. 1 (P), 5–11. http://dx.doi.org/10.1089/soro.2013.000.

Majidi, C., O'Reilly, O.M., Williams, J.A., 2012. On the stability of a rod adhering to a rigid surface: shear-induced stable adhesion and the instability of peeling. J. Mech. Phys. Solids 60 (5), 827–843. http://dx.doi.org/10.1016/j.jmps.2012.01.015.

Majidi, C., O'Reilly, O.M., Williams, J.A., 2013. Bifurcations and instability in the adhesion of intrinsically curved rods. Mech. Res. Commun. 49 (0), 13–16. http://dx.doi.org/10.1016/j.mechrescom.2013.01.004.

Majidi, C., Shepherd, R.F., Kramer, R., Whitesides, G.M., Wood, R.J., 2013. Influence of surface traction on soft robot undulation. Int. J. Rob. Res. 32 (13), 1577–1584. http://dx.doi.org/10.1177/0278364913498432.

Mosadegh, B., Polygerinos, P., Keplinger, C., Wennstedt, S., Shepherd, R.F., Gupta, U., Shim, J., Bertoldi, K., Walsh, C.J., Whitesides, G.M., 2014. Pneumatic networks for soft robotics that actuate rapidly. Adv. Funct. Mater. 24 (15), 18809–18814. http://dx.doi.org/10.1002/adfm.2013032887.

O'Reilly, O.M., Tresierras, T.N., 2011. On the evolution of intrinsic curvature in rod-based models of growth in long slender plant stems. Int. J. Solids Struct. 48 (9), 1239–1247. http://dx.doi.org/10.1016/j.ijsolstr.2010.12.006.

Seok, S., Onal, C., Wood, R.J., Rus, D., Kim, S., 2013. Meshworm: a peristaltic soft robot with antagonistic nickel titanium coil actuators. IEEE/ASME Trans. Mech. 18 (5), 1485–1497. http://dx.doi.org/10.1109/TMECH.2012.2204070.

Shepherd, R., Stokes, A., Freake, J., Barber, J., Snyder, P., Mazzeo, A., Cademartiri, L., Morin, S., Whitesides, G., 2013. Using explosions to power a soft robot. Angew. Chem. Int. Ed. 52 (10), 2892–2896. http://dx.doi.org/10.1002/anie.201209540.

Shepherd, R.F., Ilievski, F., Choi, W., Morin, S.A., Stokes, A.A., Mazzeo, A.D., Chen, X., Wang, M., Whitesides, G.M., 2011. Multigait soft robots. Proc. Nat. Acad. Sci., U.S.A. 108 (51), 20400–20403. http://dx.doi.org/10.1073/pnas.1116564108.

Song, S., Sitti, M., 2014. Soft grippers using micro-fibrillar adhesives for transfer printing. Adv. Mater 26 (28), 4901–4906. http://dx.doi.org/10.1002/adma.2014006308.

Suzumori, K., 1996. Elastic materials producing compliant robots. Rob. Auton. Syst. 18, 135–140. http://dx.doi.org/10.1016/0921-8890(95)00078-X.

Suzumori, K., Endo, S., Kanda, T., Kato, N., Suzuki, H., 2007. A bending pneumatic rubber actuator realizing soft-bodied manta swimming robot. IEEE Int. Conf. Rob. Automat., 4975–4980 http://dx.doi.org/10.1109/ROBOT.2007.364246.

Takashima, K., Noritsugu, T., Rossiter, J., Guo, S., Mukai, T., 2011. Development of curved type pneumatic artificial rubber muscle using shape-memory polymer. SICE Annu. Conf. (SICE), 1691–1695.

Trivedi, D., Rahn, C.D., Kier, W.M., Walker, I.D., 2008. Soft robotics: biological inspiration, state of the art, and future research. Appl. Bionics Biomech. 5 (3), 99–117. http://dx.doi.org/10.1080/11762320802557865.

Wakimoto, S., Ogura, K., Nishioka, Y., 2009. Miniature soft hand with curling rubber pneumatic actuators. IEEE Int. Conf. Rob. Automat., 556–561 http://dx.doi.org/10.1109/ROBOT.2009.5152259.

Zhou, X., Majidi, C., O'Reilly, O.M. Flexing in motion: a locomotion mechanism for soft robots. Int. J. Non-Linear Mech. (in press). doi: 10.1016/j.ijnonlinmec.2015.03.001.